Journal of Structural Engineering & Applied Mechanics Volume 9 Issue 2 (2026) 706

Contents lists available at https://www.goldenlightpublish.com/journals/jseam/1-toc

Journal of Structural Engineering & Applied Mechanics

Journal homepage: https://www.goldenlightpublish.com/journals/1/jseam

An elastic orthotropic punch problem in a functionally graded orthotropic layer and orthotropic half-plane system

Mohamed Hassan Ali[1], Pembe Merve Karabulut[1,*]

[1] Cankırı Karatekin University, Engineering Faculty, Department of Civil Engineering, Çankırı, Türkiye

[*] Corresponding author: P.M. Karabulut (pembemervekarabulut@karatekin.edu.tr)

https://doi.org/10.31462/jseam.2026.706

Received 4 April 2026; Revised 2 July 2026; Accepted 3 July 2026; Available online 5 July 2026

Keywords

Contact mechanics
Finite Element Method
Functionally graded materials
Orthotropic material
Elastic punch

Abstract

In this study, the frictionless receding contact problem of a functionally graded (FG) orthotropic layer, orthotropic punch, and half-plane system was investigated using the finite element method (FEM). Numerous contact mechanics problems have been solved using singular integral equations in literature. In these studies, to simplify the mathematical solution, the punch transferring the load was assumed to be rigid and its deformations were neglected. However, assuming the punch to be rigid is an idealized situation, and materials deform under load. As a result, some changes are expected in both the contact stresses and lengths, and the behavior of the entire system. The results obtained in this study were compared with other results obtained in the literature, assuming a rigid punch. The effect of punch stiffness on stress and strain was examined. The aim of this study is to contribute new results for elastic punch problems to the existing literature.

1. Introduction

Contact mechanics is the branch of science that studies the stresses, deformations, and motions in areas where two or more solid objects come into contact. This contact can be static or dynamic. Contact mechanics is critical to many engineering fields. The stresses and deformations occurring at contact surfaces determine the life, safety, and efficiency of machines, devices, and structures. Gears in mechanical engineering, tire-to-ground contact, brake systems, and landing gear in automotive and aerospace, microscale contacts and microsensors in electronics, joint mechanics and prosthetic contact in biomechanics, structure-to-ground interaction in civil engineering, and friction and wear in tribology are just some of the applications of this important subfield of physics. This branch of physics, which remains relevant, has been a research topic for many years [1–19]. Developing computer technology, in particular, has accelerated research in this area by enabling the solution of complex equations for innovative materials such as FGM [20–33]. FG materials are advanced composite materials composed of two or more materials, where the material properties can vary depending on the position within the material, in order to prevent stress concentrations in the joint regions of composite materials.

Analytical methods are inadequate for solving modern engineering problems involving complex geometries and multiple physical interactions, and in this context, the finite element method plays an indispensable role in engineering design. By enabling the solution of interdisciplinary engineering problems and reducing the cost and requirements of experimental studies, FEM shortens the engineering design process and reduces design costs. Therefore, it is currently used in engineering design in many fields, particularly structural engineering, mechanical engineering, aerospace engineering, materials engineering, and biomechanics. In the field of contact mechanics, numerous studies have been published in the literature using the finite element method to verify analytically solved problems [34–37]. In addition to these, there are some elastic punch problems that have been solved by finite element method and analytical methods in recent years [38–44].

In this study, the frictionless receding contact problem of a functionally graded (FG) orthotropic layer, orthotropic punch, and half-plane system was investigated using the finite element method. Many contact mechanics problems have been solved using singular integral equations in the literature. Taking punch deformations into account in previously solved solutions using singular integral equations significantly complicates the solution. Therefore, many studies in the literature have been conducted using singular integral equations, where the punch is assumed to be rigid and the deformations are neglected. However, the rigidity of the material is an idealized situation, and in reality, materials undergo some deformation under load. It is anticipated that these deformations may have an impact on the stress and strain of the system. While idealized systems constructed with rigid punches exhibit less complex behavior than their actual counterparts, they provide researchers with insights into material behavior. In this study, orthotropy effects are considered for the elastic punch, FG layer, and half-plane in the problem investigated. The results obtained in this study were compared with other results obtained in the literature, assuming a rigid punch. The effect of punch stiffness on stress and strain was examined, and the aim of this study is to contribute new results for elastic punch problems to the existing literature. Analytical solutions in the literature were utilized to determine the appropriate mesh density and structure in the finite element solution.

2. Methodology

In the finite element method, a system with infinite degrees of freedom is decomposed into components using a finite number of interconnected simple elements. The relationship between the forces at the nodes and their displacements is established by creating a stiffness matrix. The problem geometries for the cylindrical punch and flat punch cases to be analyzed in this study are shown in Figs. 1 and 2, respectively. In the figure, C_{ij}, $(C_{ij})_p$, $(C_{ij})_{top}$, $(C_{ij})_{bottom}$, $(C_{ij})_{hp}$, P, h, a, and b represent the stiffness parameter of the layer, stiffness parameter of the elastic orthotropic punch, stiffness parameter values of the layer on the top surface, stiffness parameter values of the layer on the bottom surface, the applied external load, the thickness of the FG orthotropic layer, and the contact lengths under the punch and between the layer and the half-plane, respectively.

When creating the finite element model for the problem, the element dimensions were assumed to be finite. Preliminary analyses were conducted to determine the length L, ensuring that the stresses were sufficiently damped. L=10 m and h=1 m were used in the analyses. Load and material properties were determined based on the ratios in the relevant solution. The problem was modeled as a two-dimensional plane strain problem. The FEM geometries for both punch cases are shown in Fig. 3.

The ANSYS finite element software package was used to perform finite element analyses of the problem. To perform the analyses, the problem's geometry, material properties, boundary conditions, and analysis type must first be defined in the program. Representative finite element models for both cases are shown in Fig. 3. Because the system geometry and loading conditions are symmetrical with respect to the y-axis, only half of the problem was modeled. ANSYS finite element software lacks an interface for defining FG materials. A subprogram was developed using Ansys Parametric Design Language (APDL) software to define materials.

Various contact algorithms have been defined in ANSYS software to accurately model the interactions of independent surfaces with different mechanical properties during loading, to ensure the accurate transfer of forces in the contact area, to accurately obtain contact lengths that vary depending on the applied external load and the mechanical properties of the contacting surfaces, and to accurately model the sliding and friction behavior that may occur on contact surfaces.

In the finite element model, the contact interaction between the punch and the layered medium was defined using surface-to-surface contact elements. The deformable layers were discretized using 6-node triangular PLANE183 elements, while the contact pair was modeled using CONTA172 and TARGE169 elements. The surface-to-surface contact formulation allows accurate contact detection even when the meshes of the contacting bodies are nonconforming.

The contact problem was solved using the Augmented Lagrange contact algorithm because of its robustness and stable convergence characteristics in nonlinear contact analyses. For this formulation, the maximum allowable penetration (FTOLN) and the contact stiffness were specified to ensure stable convergence. The contact stiffness was determined automatically by Mechanical APDL based on the material properties and the characteristic element dimensions.

The nonlinear solution was considered converged when the force and displacement residuals satisfied the default convergence criteria of ANSYS. In addition, a mesh convergence study was performed by progressively refining the mesh in the contact region. When dividing the system into finite parts, a preliminary analysis was conducted to determine the appropriate mesh density. The analysis resulted in a mesh structure with denser elements in areas where stress concentrations were observed. The final mesh density was selected after confirming that further refinement produced negligible changes in the contact pressure and stress distributions. A cross-section of the system mesh is shown in Fig. 4.

The results obtained from the analysis were compared with the analytical results of the rigid punch case previously made in the literature [5,19], and it was confirmed that the results had the desired precision. The post-analysis deformed shape of the problem for both punch cases is shown in Fig. 5.

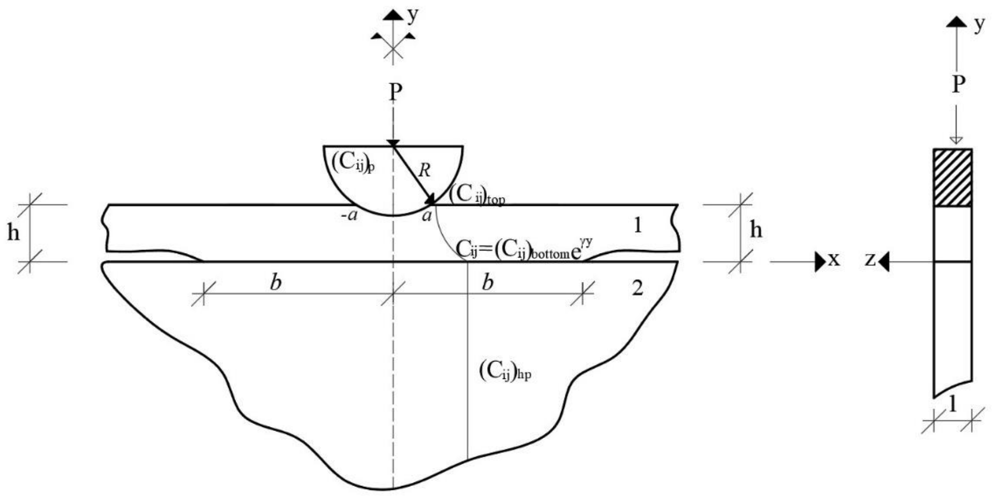

Fig. 1. Geometry of problem for cylindrical punch case

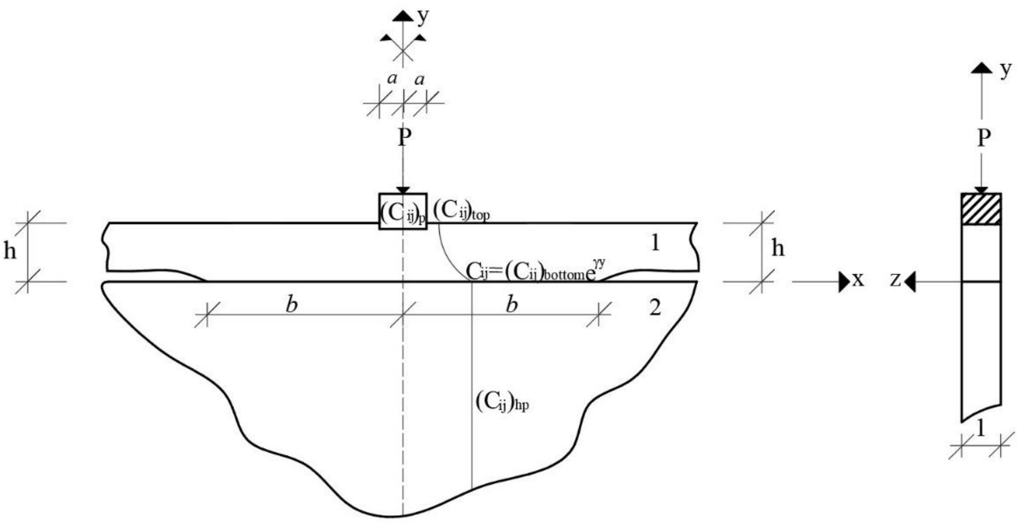

Fig. 2. Geometry of problem for flat punch case

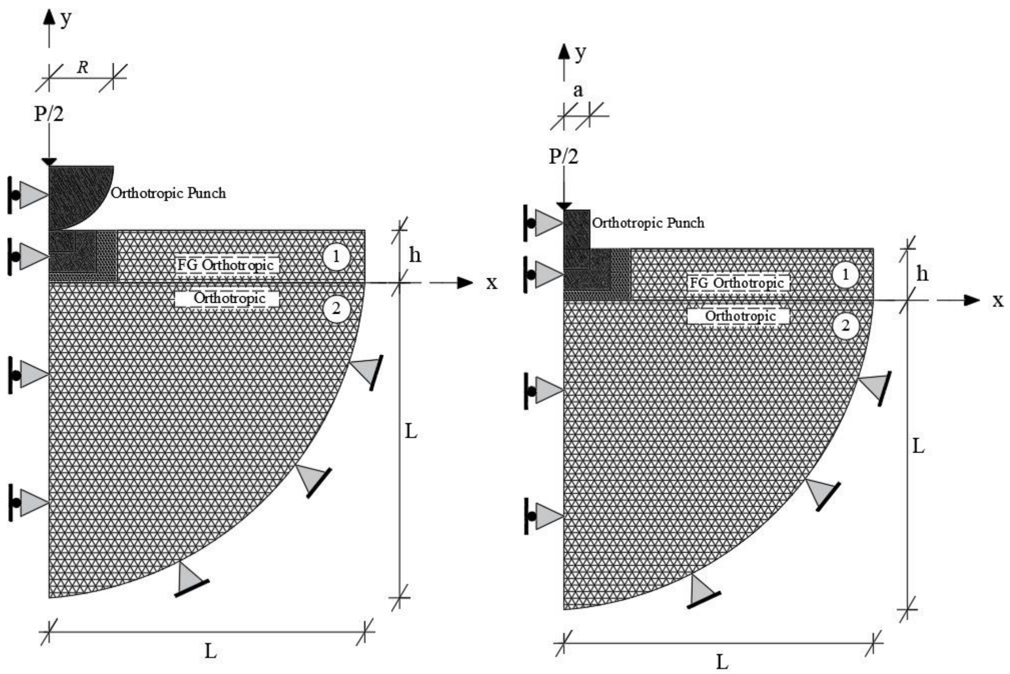

Fig. 3. Finite element model of the cylindrical and flat punch cases respectively

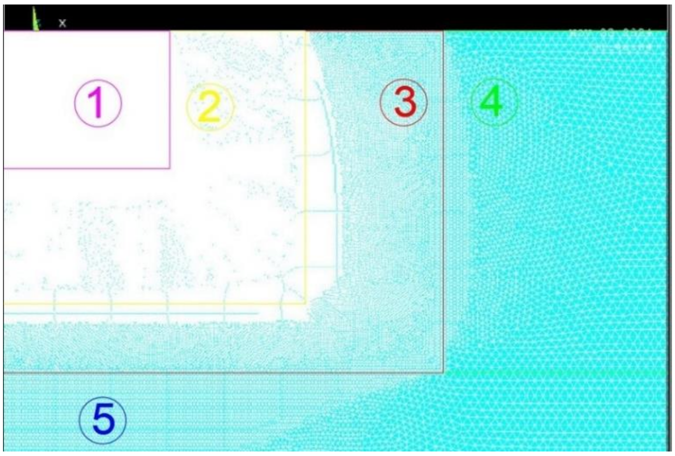

Fig. 4. Cross section of the meshed structure

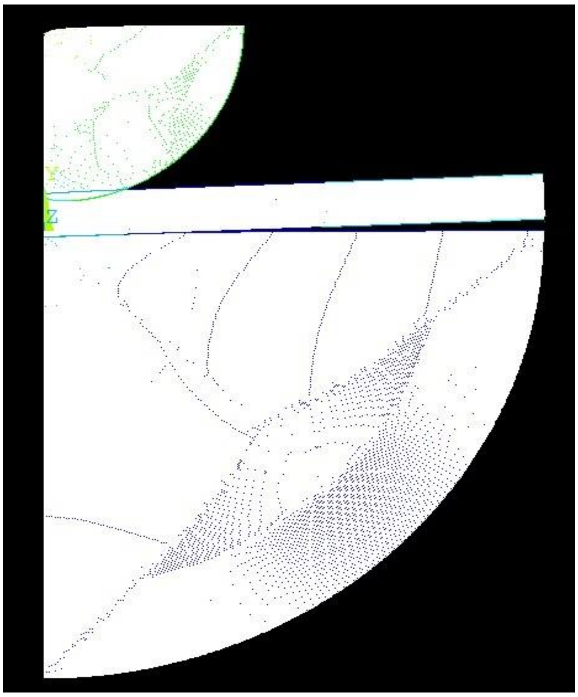

(a)

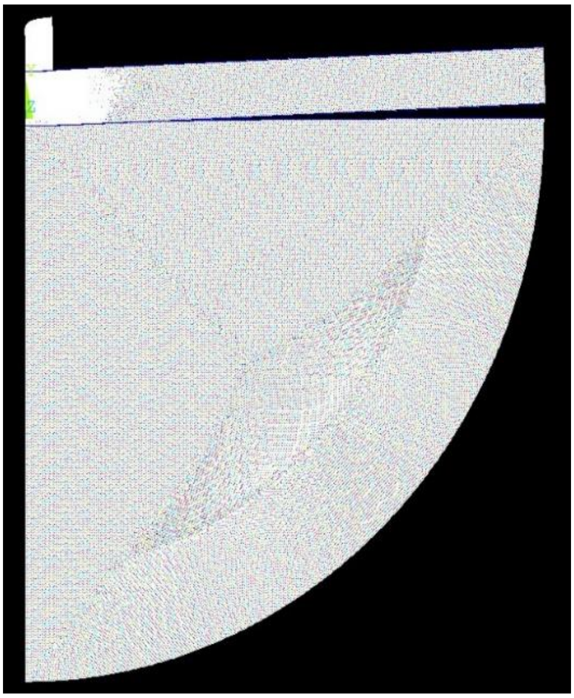

(b)

Fig. 5. Deformed shape of the problem (a) cylindrical punch case (b) flat punch case

3. Results and discussion

In this study, the frictionless receding contact problem between an orthotropic punch and an FG orthotropic layer-orthotropic half-plane system was solved using the finite element method. The effects of punch stiffness, FG layer stiffness variation, and external load on the contact stresses under the punch $p_1(x_1)$, between the layer and half-plane $p_2(x_2)$, contact lengths (a, b), horizontal $u_x(x_1, y)$, and vertical $u_y(x_1, y)$, deformations on the layer's upper surface were investigated. Separate results were obtained for the cylindrical and flat punch shapes. The results were obtained for dimensionless values. The problem was solved assuming a plane strain condition. This study utilized three different orthotropic materials found in the literature [4]. The selection of these materials did not have a specific purpose. The orthotropic material properties used in the analyses are shown in Table 1.

Table 2 presents the mesh size study for the flat punch case. After specific element dimensions, the contact lengths converge to a specific value. The initial element dimensions at which convergence occurs provide the appropriate element dimensions for the solution. Furthermore, in Figs. 6 and 11, the results from the finite element model for cylindrical and flat punch cases are compared with those from the literature [5,19] for the same geometries. The approximation of the results obtained from the finite element model for the elastic punch case with the results obtained from the analytical model for the rigid punch case is examined. It is observed that the results obtained for the special case where the punch rigidity is 10^5 times more rigid than the layer are sufficiently close to each other in terms of accuracy.

Table 1. Orthotropic material constants [4]

Material	E_{11} (GPa)	E_{22} (GPa)	E_{33} (GPa)	E_{12} (GPa)	E_{13} (GPa)	E_{23} (GPa)	ν_{12}	ν_{13}	ν_{23}
Material A (Gl/Ep)	42.7	11.7	11.7	8.238	8.238	3.778	0.27	0.27	0.55
Material B (B/Al)	227.5	137.9	137.9	55.152	55.152	49.244	0.24	0.24	0.4
Material C (Gr/Al)	402.6	24.1	24.1	16.75	16.75	8.34	0.29	0.29	0.45

Table 2. Mesh size study for flat punch case $(a/h = 2, (P/h)/(C_{55})_A = 5x10^{-3}$, $(C_{ij})_{top}/\ (C_{ij})_{bottom} = 2, (C_{ij})_{bottom}/\ (C_{ij})_{hp} = 3$, Material A)

Model Number	b/h	Number of elements	Number of nodes
1	4	1062	2126
2	3.8	6064	12115
3	3.61	26516	53043
4	3.6	41898	83856
5	3.6	210674	421514

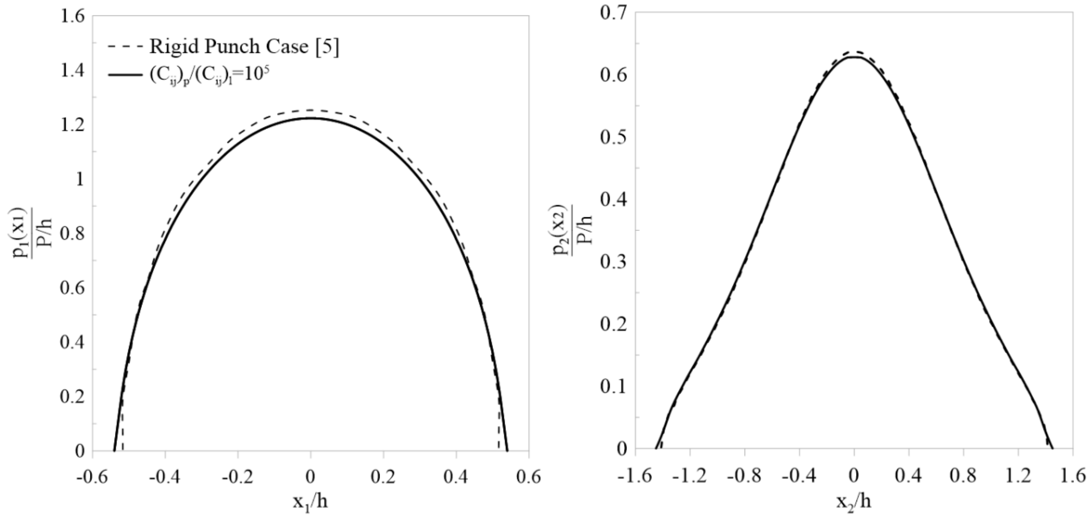

Fig. 6. Comparison of contact stresses for cylindrical punch case with Çömez [5] $(R/h = 100, C_{ij}/(C_{ij})_{hp} = 1,\ C_{55}/\ (P/h) = 200, (C_{ij})_{top}/\ (C_{ij})_{bottom} = 1$, Homogeneous isotropic special case)

Figs. 6-10 show the results obtained for the cylindrical elastic punch case, and Figs. 11-15 show the results obtained for the flat elastic punch case. Fig. 7 examines the effects of the stiffness ratio of the elastic punch and layer on the contact stresses under the punch, between the layer and the half-plane, the horizontal displacement at the top surface of the layer, and the vertical displacements, respectively. Contact stress concentrations are governed by the local contact stiffness. When the punch is much stiffer than the layer, the punch undergoes negligible deformation and forces the layer to accommodate almost the entire deformation. This results in a highly localized load transfer near the center of the contact region, producing large stress gradients and higher peak contact pressures. As the punch stiffness decreases, a larger portion of the applied load is absorbed through deformation of the punch itself. Consequently, the load is distributed over a wider contact area, reducing stress concentration and lowering the maximum contact pressure. As the punch-to-layer stiffness ratio decreases from 10^5 to 10, the maximum contact pressure beneath the punch decreases by only 7.8%. However, when the stiffness ratio is further reduced to 1 and 0.5, the peak contact pressure decreases by approximately 39.4% and 52.2%, respectively, indicating that substantial stress redistribution occurs once the punch stiffness becomes comparable to that of the layer. In contrast, the contact pressure transmitted to the layer–half-plane interface is much less sensitive to punch stiffness, exhibiting a maximum reduction of only 6.6%, even for the lowest stiffness ratio investigated. When the deformations on the upper surface of the layer are examined, it is observed that the rigid punch penetrates the layer more deeply into the layer, and there is no significant change in the x-direction deformations.

Fig. 8 illustrates the effects of the ratio of the upper surface stiffness to the lower surface stiffness of an FG orthotropic layer on the contact stresses under the punch, between the layer and the half-plane, the horizontal and vertical displacements at the upper surface of the layer, respectively. The stiffness parameters of an FG layer vary exponentially starting from the lower surface. When the upper surface of the layer is stiffer, the total stiffness of the layer increases, the punch penetrates the layer less, thus reducing contact lengths and the maximum value of contact stresses increases. As the layer becomes stiffer, it undergoes less deformation, which increases the contact length between the layer and the half-plane.

The effects of the external load ratio on the contact stresses under the punch, between the layer and the half-plane, the horizontal and vertical displacements at the top surface of the layer, respectively, are examined in Fig. 9. As can be seen from the figure, in the case of a cylindrical punch, the contact stresses and lengths under the punch increase proportionally with increasing load. The contact lengths between the layer and the half-plane do not change for the specified load ratios, but the maximum value of the contact stresses increases proportionally with increasing load values.

In Fig. 10, the effect of punch radius on the contact stresses under the punch, between the layer and the half-plane, the horizontal and vertical displacements at the top surface of the layer, respectively, are illustrated. As the punch radius increases, the contact lengths between the layer and the elastic punch increase. Since the load is small, its effect diminishes at depth, and therefore it does not significantly affect the contact stresses between the layer and the half-plane. As the external load remains constant, the horizontal and vertical displacements under the punch do not change much.

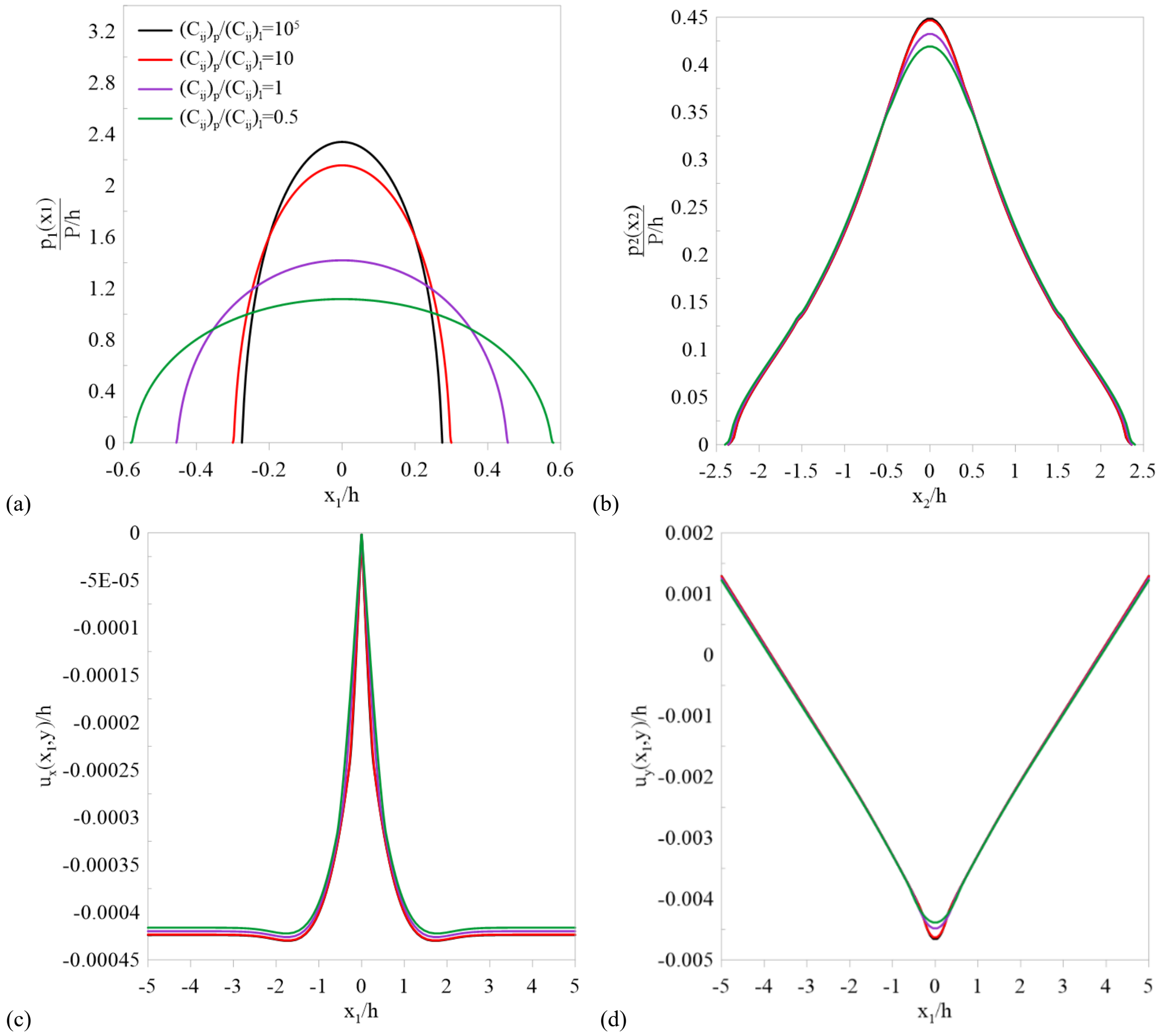

Fig. 7. Effect of the rigidity ratio on (a) the contact pressure beneath the punch, (b) the contact pressure at the layer–half-plane interface, (c) the horizontal displacement beneath the punch, and (d) the vertical displacement beneath the punch for the isotropic case (Material B; cylindrical punch; (Material B; cylindrical punch; $R/h = 100$; $(P/h)/(C_{55})_A = 10^{-2}$; $(C_{ij})_{\text{top}}/(C_{ij})_{\text{bottom}} = 2$; $(C_{ij})_{\text{bottom}}/(C_{ij})_{\text{hp}} = 3$; and $\left(C_{ij}\right)_p/C_{ij} = 1$)

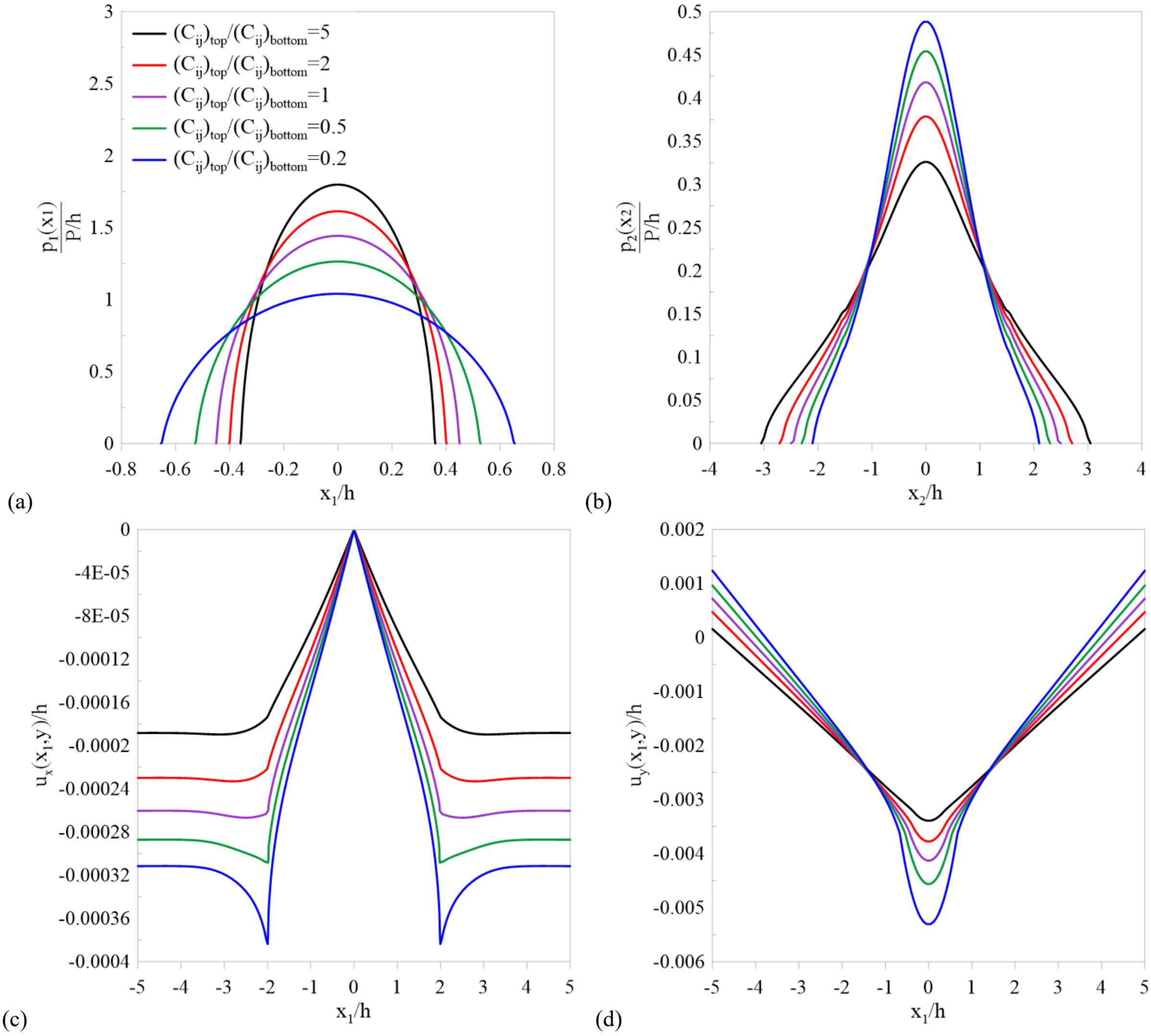

Fig. 8. Effect of the top-to-bottom rigidity ratio in the functionally graded orthotropic layer on (a) the contact pressure beneath the punch, (b) the contact pressure at the layer–half-plane interface, (c) the horizontal displacement beneath the punch, and (d) the vertical displacement beneath the punch (Material A; cylindrical punch; ; $(P/h)/(C_{55})_A = 5\times10^{-3}$; $(C_{ij})_{\mathrm{bottom}}/(C_{ij})_{\mathrm{hp}} = 3$; and $(C_{ij})_p/C_{ij} = 1$)

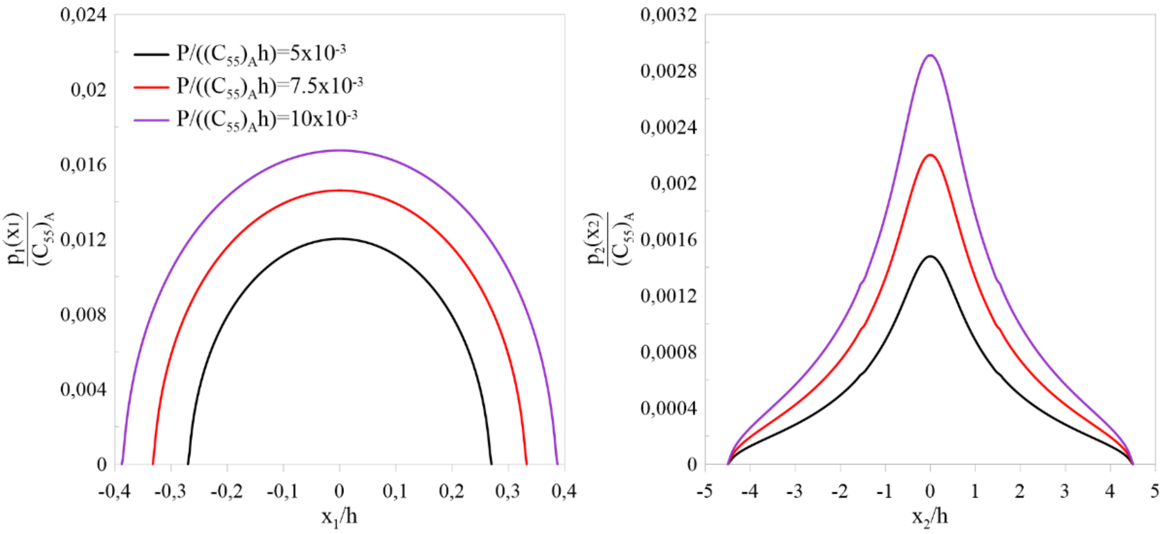

Fig. 9. Effect of the external load ratio on (a) the contact pressure beneath the punch, (b) the contact pressure at the layer–half-plane interface, (c) the horizontal displacement beneath the punch, and (d) the vertical displacement beneath the punch (Material C; cylindrical punch; $R/h = 100$; $(C_{ij})_{\mathrm{bottom}}/(C_{ij})_{\mathrm{hp}} = 3$; and $(C_{ij})_p/C_{ij} = 1$)

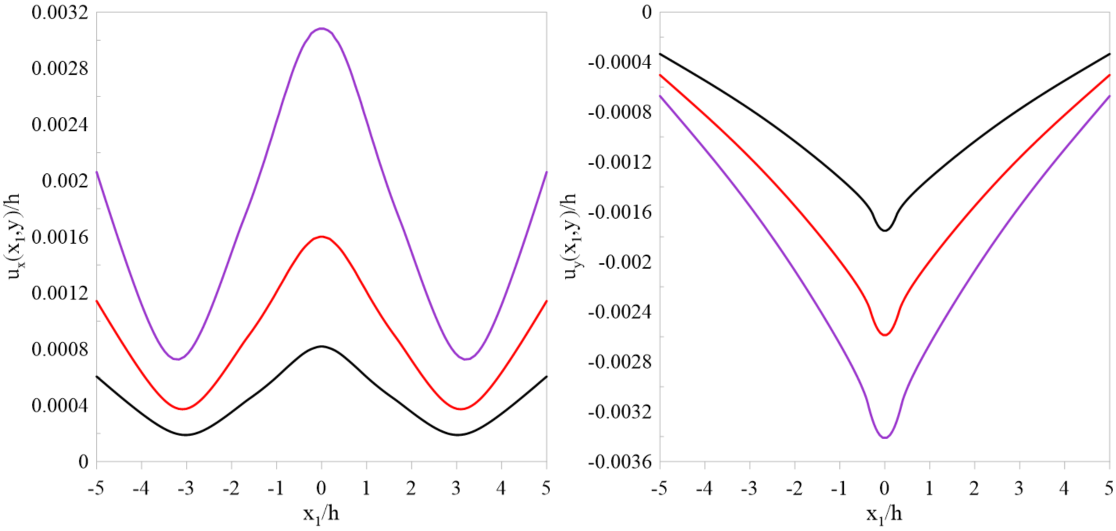

Fig. 9. Continued

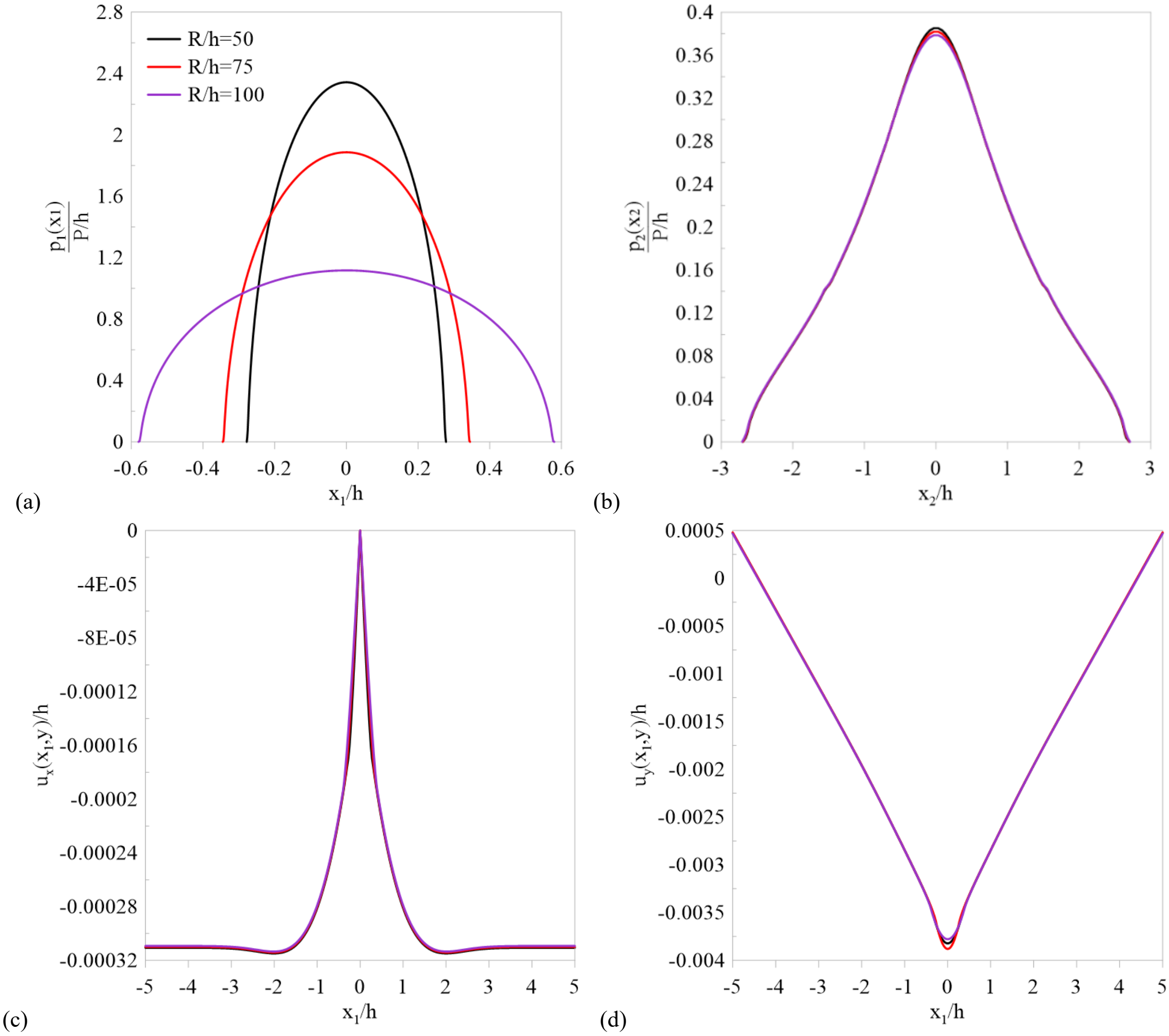

Fig. 10. Effect of the punch radius on (a) the contact pressure beneath the punch, (b) the contact pressure at the layer–half-plane interface, (c) the horizontal displacement beneath the punch, and (d) the vertical displacement beneath the punch (Material A; cylindrical punch; $P/h)/(C_{55})_A = 5 \times 10^{-3}$; $(C_{ij})_{\text{top}}/(C_{ij})_{\text{bottom}} = 2$; $(C_{ij})_{\text{bottom}}/(C_{ij})_{\text{hp}} = 3$; and $(C_{ij})_p/C_{ij} = 1$)

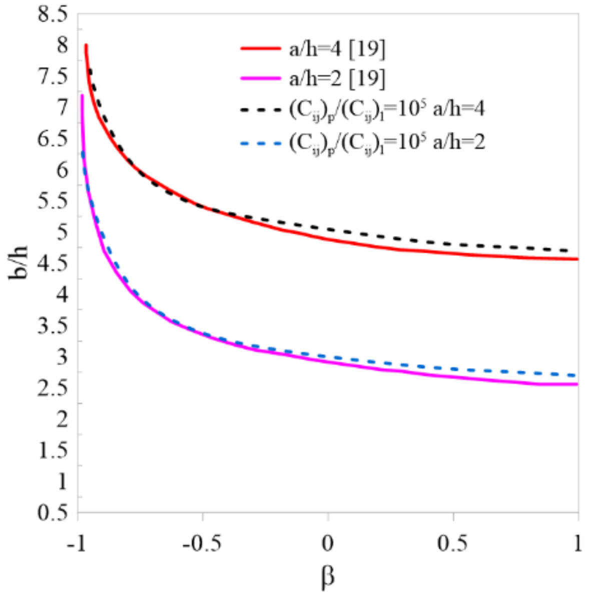

Fig. 11. Comparison of contact lengths for flat punch with Ratwani and Erdoğan [19] $\left(\beta = \frac{(4-4\nu_l)(C_{55})_{hp}-(4-4\nu_{hp})(C_{55})_l}{(4-4\nu_l)(C_{55})_{hp}+(4-4\nu_{hp})(C_{55})_l};\ \frac{(C_{ij})_{\text{top}}}{(C_{ij})_{\text{bottom}}} = 1;\ \text{Homogeneous isotropic case}\right)$

Fig. 11 shows contact lengths of the contact lengths for the flat punch case with Ratwani and Erdoğan [19]. For the homogeneous isotropic special case, where the punch is 10^5 times more rigid than the layer, the results obtained from the finite element model for the elastic punch converge to the results obtained from the analytical solution assuming the punch is rigid.

Fig.12 examines the effects of the ratio of the stiffness of the elastic punch and the layer on the contact stresses under the punch, between the punch and the half-plane, the horizontal and vertical displacement on the layer's upper surface, respectively. Although the maximum contact pressure beneath the flat punch remains nearly unchanged for all cases, the pressure distribution changes considerably near the symmetry axis. At x=0, the contact pressure increases by approximately 34.6%, 194.8%, and 261.7% relative to the reference case. This indicates that the variation in stiffness ratio mainly alters the load-sharing mechanism within the contact region rather than simply changing the peak pressure. Unlike the contact pressure beneath the punch, the contact pressure at the layer–half-plane interface exhibits a delayed response to changes in stiffness ratio. The maximum interface pressure changes by only 13% between the first two cases but increases by 64% and 84% in the remaining cases. When the punch stiffness decreases, the punch no longer behaves as an undeformable body capable of maintaining a perfectly flat contact surface. Instead, the punch itself bends under the applied load. Owing to its finite bending stiffness, the central region undergoes larger vertical deformation than the regions closer to the free edges. Consequently, the initially flat contact surface gradually adopts a curved profile, producing a deformation pattern similar to that of a cylindrical punch. This deformation alters the contact pressure distribution, demonstrating that the resulting deformation profile depends not only on the initial punch geometry but also on the relative bending stiffness of the punch. Furthermore, unlike the cylindrical punch case, the horizontal and vertical displacements on the upper surface of the layer change considerably for the same material and load ratios. The values of horizontal displacement and the peak values of vertical displacement increase significantly with decreasing stiffness ratio. While the change in horizontal displacements on the upper surface of the layer is zero under the rigid-punch assumption, with decreasing stiffness ratios, the vertical displacements under the punch become cylindrical rather than parallel to the punch shape.

Fig. 13 examines the effect of changing the ratio of the stiffness of the upper surface to the lower surface of an FG orthotropic layer on the contact stresses under the punch, between the layer and the half-plane, the horizontal and vertical displacements on the upper surface of the layer, respectively. Accordingly, with increasing layer stiffness, the values of the contact stresses under the punch do not change significantly, while the values on the axis of symmetry decrease slightly. The peak values of the contact stresses between the layer and the half-plane increase and contact lengths decrease with this change. Although larger deformations occur on the upper surface of the layer on the axis of symmetry as the layer stiffness decreases, the deformations continue to be effective in the rigid layer case in more distant regions.

The effect of external load on the contact stresses under the punch, between the layer and the half-plane, the horizontal and vertical displacement on the upper surface of the layer are examined in Fig. 14. As can be seen from the figure, in the case of a flat punch, the contact stresses under the punch increase proportionally with the external load. For the specified load ratios, while the contact lengths between the layer and the half-plane remain unchanged, the value of the contact stresses increases proportionally with the load, and the deformations on the upper surface of the layer increase with the increasing load ratios.

The effect of punch width on the contact pressures under the punch and between the layer and half plane, horizontal displacement and vertical displacement under the punch respectively is investigated in Fig. 15. As the punch width increases, the stress spread over a wider area, thus significantly reducing the contact stress values and horizontal and vertical deformations on the upper surface of the layer.

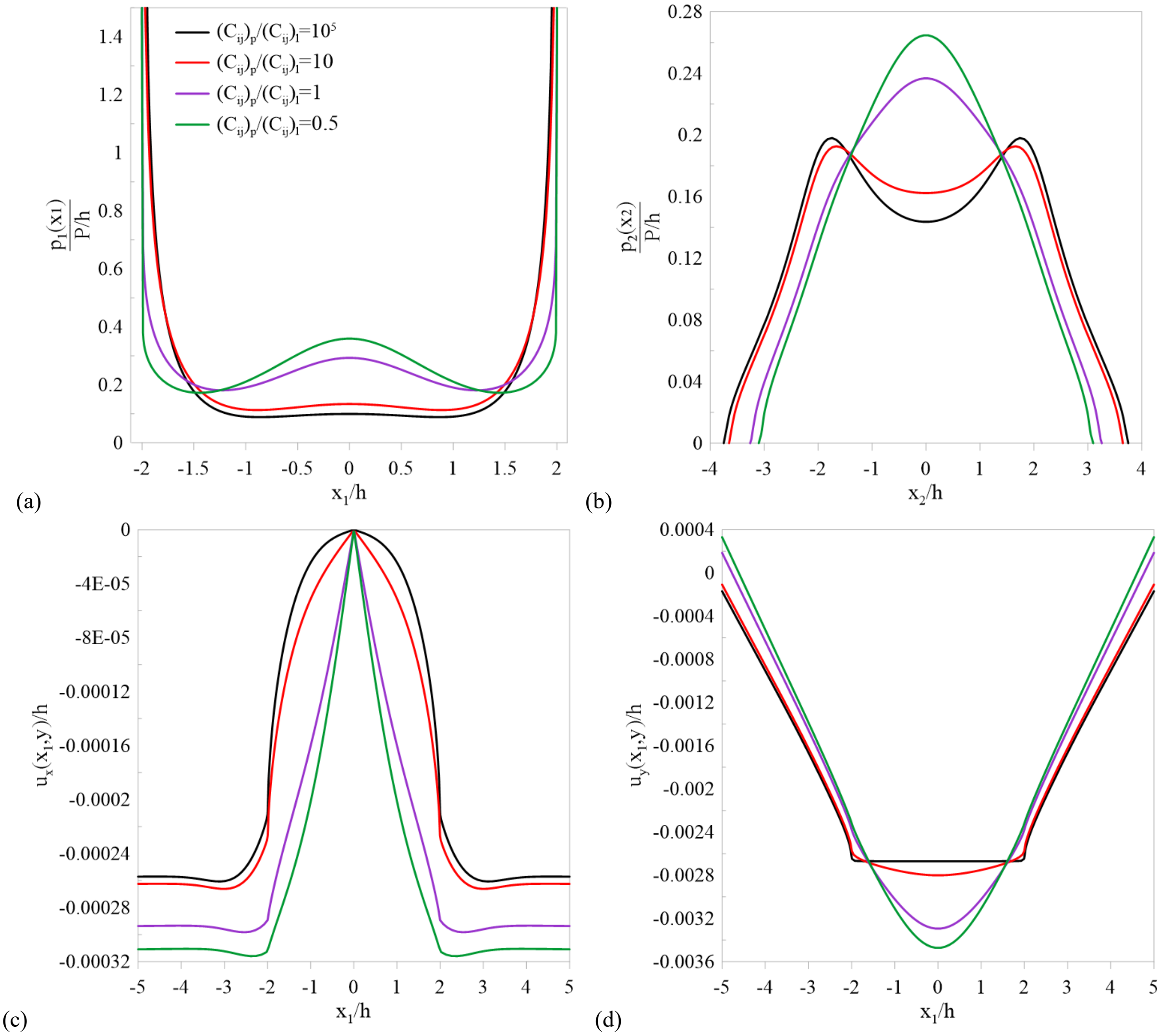

Fig. 12. Effect of the layer-to-punch rigidity ratio on (a) the contact pressure beneath the punch, (b) the contact pressure at the layer–half-plane interface, (c) the horizontal displacement beneath the punch, and (d) the vertical displacement beneath the punch for the isotropic case (Material B; flat punch; $a/h = 2$; $(P/h)/(C_{55})_A = 10^{-2}$; $(C_{ij})_{\text{top}}/(C_{ij})_{\text{bottom}} = 2$; and $(C_{ij})_{\text{bottom}}/(C_{ij})_{\text{hp}} = 3$)

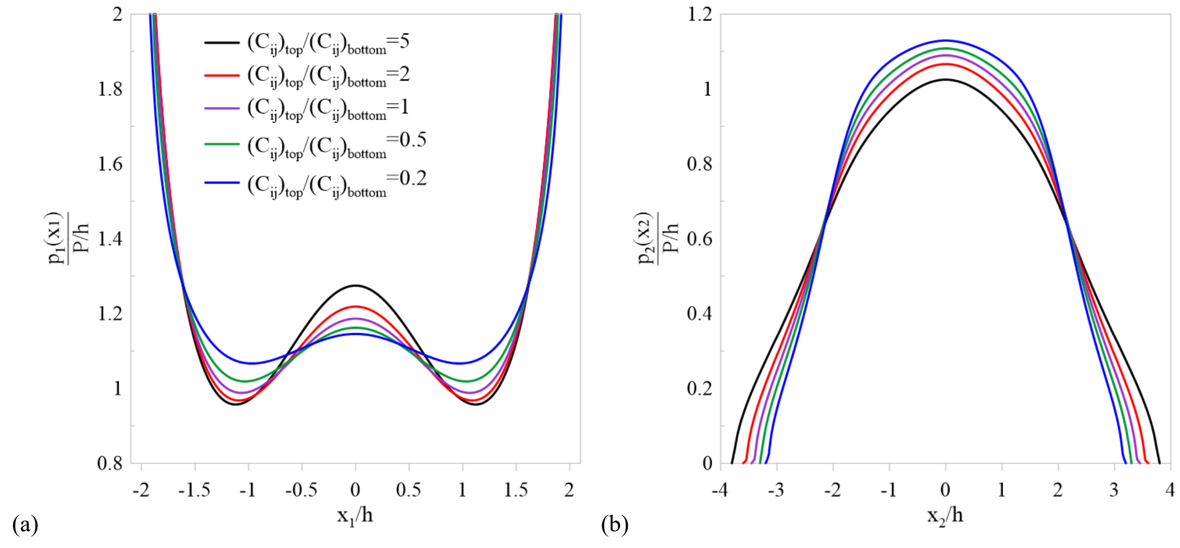

Fig. 13. Effect of the top-to-bottom rigidity ratio in the functionally graded orthotropic layer on (a) the contact pressure beneath the punch, (b) the contact pressure at the layer–half-plane interface, (c) the horizontal displacement beneath the punch, and (d) the vertical displacement beneath the punch (Material A; flat punch; $a/h = 2$; $(P/h)/(C_{55})_A = 5 \times 10^{-3}$; $(C_{ij})_{\text{bottom}}/(C_{ij})_{\text{hp}} = 3$; and $(C_{ij})_p/C_{ij} = 1$)

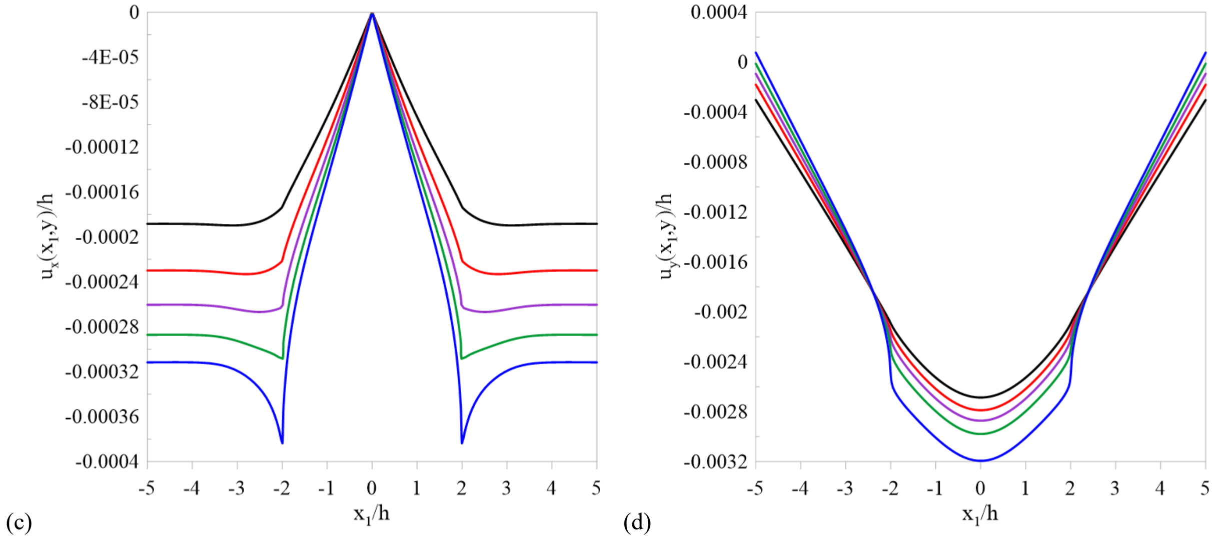

Fig. 13. Continued

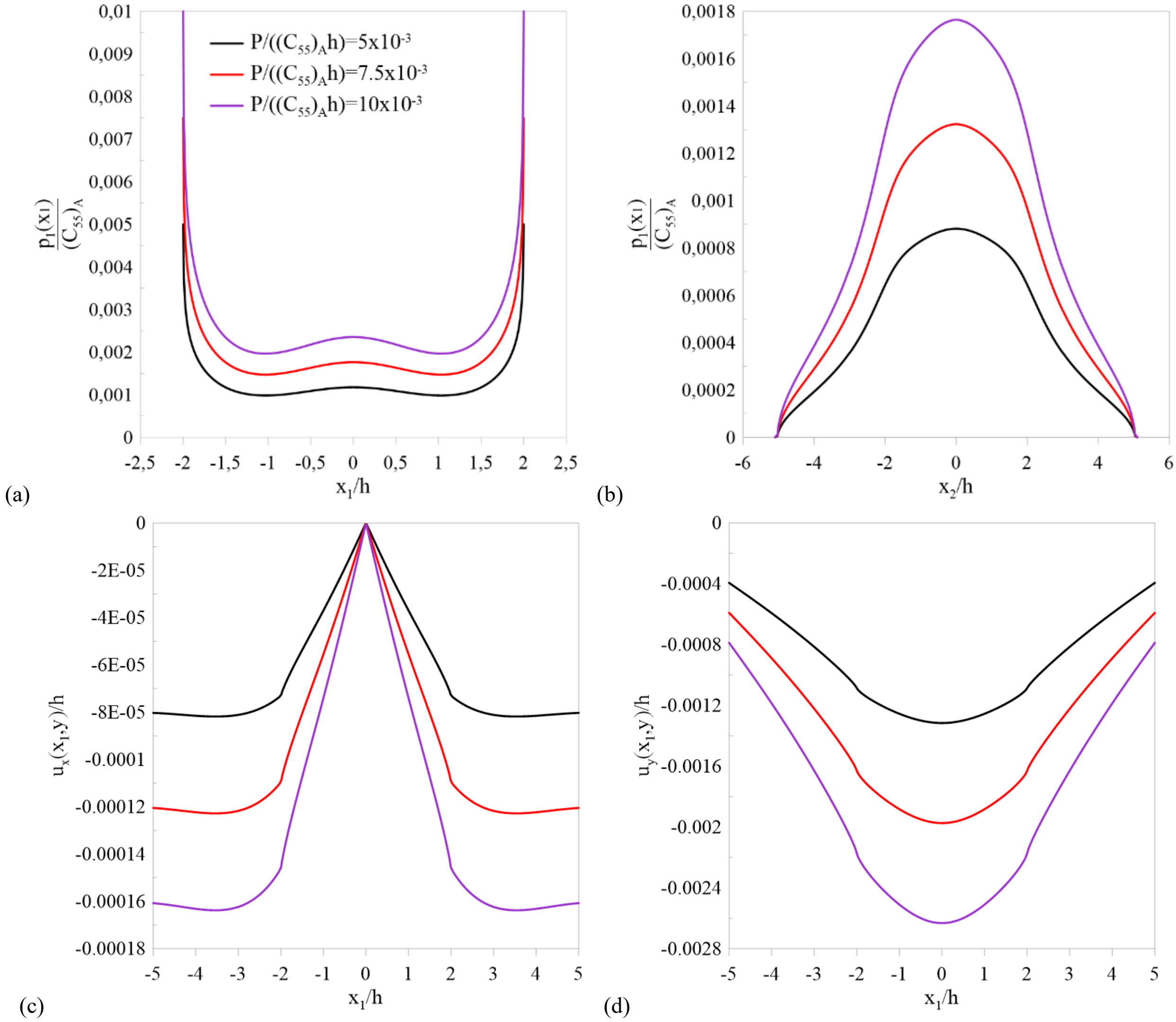

Fig. 14. Effect of the external load ratio on (a) the contact pressure beneath the punch, (b) the contact pressure at the layer–half-plane interface, (c) the horizontal displacement beneath the punch, and (d) the vertical displacement beneath the punch (Material C; flat punch; $a/h = 2$; $(C_{ij})_{\text{top}}/(C_{ij})_{\text{bottom}} = 2$; $(C_{ij})_{\text{bottom}}/(C_{ij})_{\text{hp}} = 3$; and $(C_{ij})_p/C_{ij} = 1$)

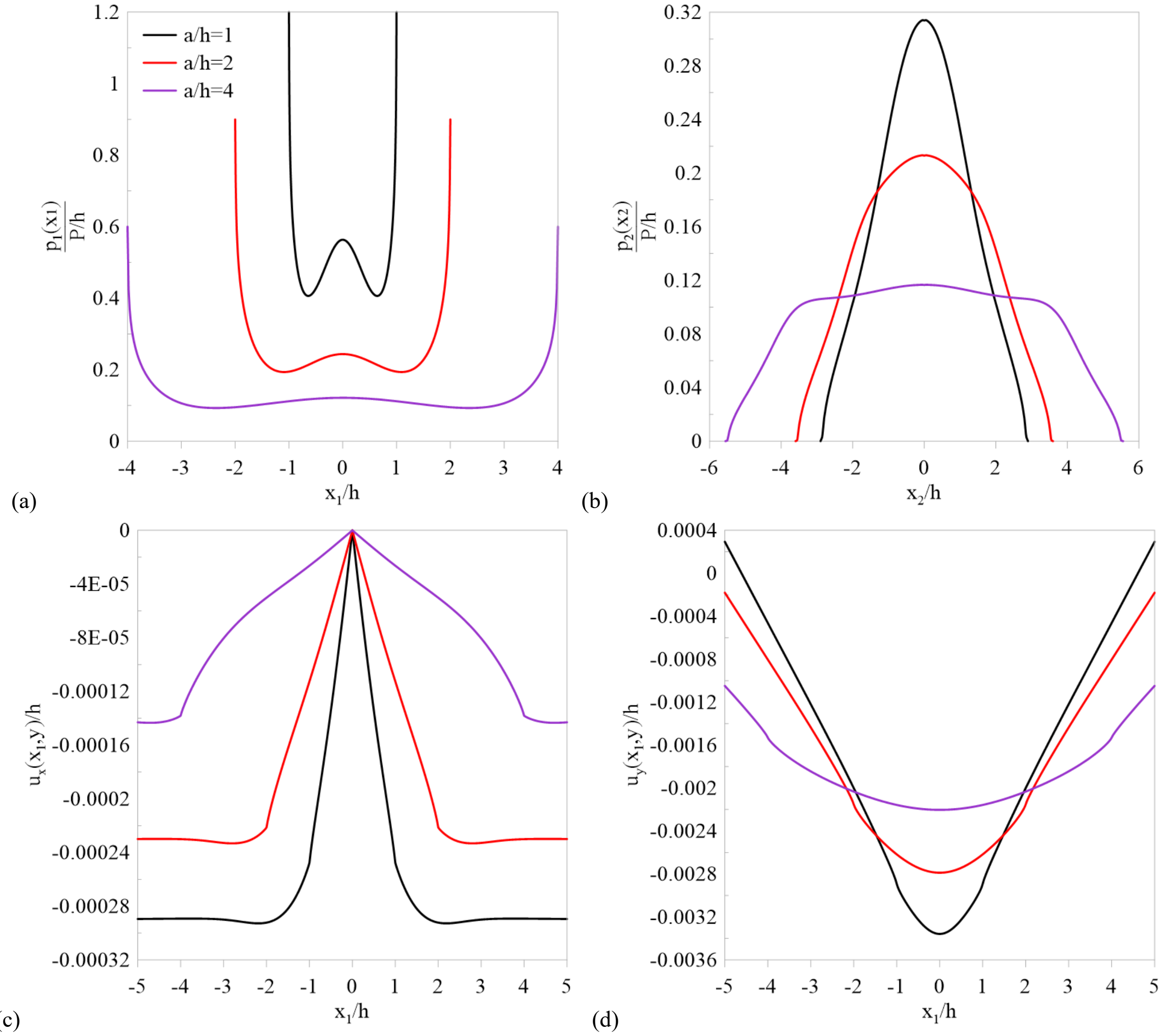

Fig. 15. Effect of the punch width on (a) the contact pressure beneath the punch, (b) the contact pressure at the layer–half-plane interface, (c) the horizontal displacement beneath the punch, and (d) the vertical displacement beneath the punch (Material A; flat punch; $(P/h)/(C_{55})_A = 5 \times 10^{-3}$; $(C_{ij})_{\text{top}}/(C_{ij})_{\text{bottom}} = 2$; $(C_{ij})_{\text{bottom}}/(C_{ij})_{\text{hp}} = 3$; and $(C_{ij})_p/C_{ij} = 1$)

4. Conclusions

In this study, the frictionless receding-contact problem involving an orthotropic punch, a functionally graded layer, and an orthotropic half-plane was investigated using the finite element method. The results show that, for both cylindrical and flat punches, the contact stresses, contact lengths, and displacements obtained when the punch stiffness is 10^5 times greater than that of the layer converge to the corresponding analytical solutions based on the rigid-punch assumption. As the punch stiffness decreases, however, substantial changes occur in the contact stresses, contact lengths, and displacement distributions, demonstrating that punch deformability has a significant influence on the overall contact response.

The cylindrical and flat punches exhibit different deformation characteristics. Under loading, the flat punch deforms and therefore no longer strictly satisfies the analytical boundary condition requiring a constant vertical displacement beneath the punch. Moreover, convergence to the rigid-punch solution is achieved at lower stiffness ratios for the cylindrical punch than for the flat punch. The stiffness variation within the functionally graded layer also has a pronounced effect on the contact behavior. Increasing the stiffness of the upper region of the layer reduces the surface deformations and the contact length beneath the cylindrical punch, while increasing the contact length at the interface between the functionally graded layer and the half-plane. For both punch geometries, increasing the applied load leads to higher contact stresses and larger displacements.

Accounting for punch elasticity provides a more realistic representation of contact stresses, contact lengths, and deformation because the mechanical response of the punch is included directly in the analysis. This approach therefore offers results that are more representative of practical engineering systems and enables the effects of punch stiffness, stress distribution, and material properties to be evaluated. Nevertheless, the elastic-punch formulation is more complex than the rigid-punch idealization, both analytically and numerically, and convergence difficulties may arise in finite element simulations.

The present study extends the existing literature, which has largely relied on the rigid-punch assumption, by demonstrating the influence of punch deformability and graded-layer design on the mechanical response of orthotropic contact systems. The findings provide useful guidance for the analysis and design of functionally graded and orthotropic structural components. Future studies may extend the proposed framework to include frictional contact, dynamic and cyclic loading, thermal effects, piezoelectric coupling, viscoelastic or plastic material behavior, and three-dimensional punch geometries. Such developments would improve the applicability of the model to engineering fields including laminated composites, biomechanics, and structural mechanics.

Appendix

The expressions of the coefficients C_{ij} in Eqs. (1) can be expressed as follows by the engineering constants [45]:

$$C_{11} = \frac{1-\nu_{23}\nu_{32}}{E_2E_3\Delta}, \quad C_{13} = \frac{\nu_{31}+\nu_{21}\nu_{32}}{E_2E_3\Delta},$$

$$C_{33} = \frac{1-\nu_{12}\nu_{21}}{E_1E_2\Delta}, \quad C_{55} = G_{31}$$

where

$$\Delta = \frac{1-\nu_{12}\nu_{21}-\nu_{23}\nu_{32}-\nu_{31}\nu_{13}-2\nu_{21}\nu_{32}\nu_{13}}{E_1E_2E_3}$$

and ν_{ij} is the Poisson' ratio, E_1 E_2 and E_3 are Young' moduli, and G_{31} is the shear modulus.

Declarations

Conflict of interests

The author(s) declared no potential conflicts of interest with respect to the research, authorship, and/or publication of this article.

Funding

This research received no external funding.

Author contributions

All authors contributed equally to this study. All authors have read and approved of the final manuscript and accept equal responsibility for its content.

Data availability statement

The data presented in this study are available on request from the corresponding author.

Use of generative AI and AI-assisted technologies

The author(s) confirm the author(s) did not use any AI tools in the preparation of this work/research/study.

References

[1] Aleksandrov VM (2006) Two problems with mixed boundary conditions for an elastic orthotropic strip. J Appl Math Mech 70:128–138.

[2] Ballard P (2013) Steady sliding frictional contact problems in linear elasticity. J Elast 110:33–61.

[3] Benjumea R, Sikarskie DL (1972) On the solution of plane, orthotropic elasticity problems by an integral method. J Appl Mech 39:801–808.

[4] Binienda WK, Pindera M-J (1994) Frictionless contact of layered metal-matrix and polymer-matrix composite half planes. Compos Sci Technol 50:119–128.

[5] Çömez İ (2010) Frictional contact problem for a rigid cylindrical stamp and an elastic layer resting on a half plane. Int J Solids Struct 47:1090–1097.

[6] Çömez İ, Karabulut PM (2022) Continuous and discontinuous contact problem of a magneto-electro-elastic layer. Struct Eng Mech 83:67–77.

[7] Falope FO, Radi E (2016) Finite thin cover on an orthotropic elastic half plane. Model Simul Eng 2016:5393621.

[8] Karabulut PM, Çetinkaya İT, Oğuz H, Çömez İ (2024) Moving contact problem of a functionally graded orthotropic coated half plane. Acta Mech 235:3989–4004.

[9] Lopes JP, Hills DA (2019) The axisymmetric frictional receding contact of a layer pressed against a half-space by a point force. Int J Solids Struct 171:47–53.

[10] Oğuz H, Çetinkaya İT, Çömez İ (2024) Receding contact problem of an orthotropic layer supported by rigid quarter planes. Struct Eng Mech 91:459–468.

[11] Oğuz H, Çetinkaya İT, Çömez İ (2024) Frictional receding contact problem of a functionally graded orthotropic layer / orthotropic interlayer / isotropic half plane system. J Mech Mater Struct 19:651–667.

[12] Öner E (2021) Two-dimensional frictionless contact analysis of an orthotropic layer under gravity. J Mech Mater Struct 16:573–594.

[13] Öner E (2021) Frictionless contact mechanics of an orthotropic coating/isotropic substrate system. Comput Concr 28:209–220.

[14] Parel KS (2021) Plane frictional receding contact of a thin layer pressed onto a substrate by finite pressure distributions. Eur J Mech - ASolids 90:104309.

[15] Pozharskii DA (2017) Contact problem for an orthotropic half-space. Mech Solids 52:315–322.

[16] Slobodyan BS, Lyashenko BA, Malanchuk NI, Marchuk VE, Martynyak RM (2016) Modeling of contact interaction of periodically textured bodies with regard for frictional slip. J Math Sci 215:110–120.

[17] Shen JJ, Wu YY, Lin JX, Xu FY, Li CG (2018) Partial slip problem in frictional contact of orthotropic elastic half-plane and rigid punch. Int J Mech Sci 135:168–175.

[18] Üstün A, Adıyaman G, Özşahin TŞ (2023) Analytical solution for contact and crack problem ın homogeneous half-plane. Arch Appl Mech 93:4399–4423.

[19] Ratwani M, Erdogan F (1973) On the plane contact problem for a frictionless elastic layer. Int J Solids Struct 9:921–936.

[20] Alinia Y, Espo M (2020) Sliding contact problem of an FGM coating/substrate system with two-dimensional material property grading. Acta Mech 231:649–659.

[21] Attia MA, El-Shafei AG (2020) Investigation of multibody receding frictional indentation problems of unbonded elastic functionally graded layers. Int J Mech Sci 184:105838.

[22] Cao R, Li L, Li X, Mi C (2021) On the frictional receding contact between a graded layer and an orthotropic substrate indented by a rigid flat-ended stamp. Mech Mater 158:103847.

[23] Chen P, Chen S (2012) Contact behaviors of a rigid punch and a homogeneous half-space coated with a graded layer. Acta Mech 223:563–577.

[24] Chen P, Chen S, Peng J (2015) Frictional contact of a rigid punch on an arbitrarily oriented gradient half-plane. Acta Mech 226:4207–4221.

[25] Chen P, Chen S, Peng J (2015) Sliding contact between a cylindrical punch and a graded half-plane with an arbitrary gradient direction. J Appl Mech Trans ASME 82.

[26] Chidlow SJ, Teodorescu M (2014) Sliding contact problems involving inhomogeneous materials comprising a coating-transition layer-substrate and a rigid punch. Int J Solids Struct 51:1931–1945.

[27] Elloumi R, Kallel-Kamoun I, El-Borgi S (2010) A fully coupled partial slip contact problem in a graded half-plane. Mech Mater 42:417–428.

[28] Gun H, Gao X-W (2014) Analysis of frictional contact problems for functionally graded materials using BEM. Eng Anal Bound Elem 38:1–7.

[29] Guler MA, Erdogan F (2007) The frictional sliding contact problems of rigid parabolic and cylindrical stamps on graded coatings. Int J Mech Sci 49:161–182.

[30] Jobin KJ, Abhilash MN, Murthy H (2017) A simplified analysis of 2D sliding frictional contact between rigid indenters and FGM coated substrates. Tribol Int 108:174–185.

[31] Owoputi AO, Inambao FL, Ebhota WS (2018) A review of functionally graded materials: fabrication processes and applications. Presented at the.

[32] Tian X, Zhou Y, Ding S, Wang L (2024) Exploring the effects of finite size and indenter shape on the contact behavior of functionally graded thermoelectric materials. Int J Solids Struct 305:113089.

[33] Tian X, Zhou Y, Zhang C (2025) The reliability of elastic electrode/graded thermoelectric substrate systems with the adhesive interlayer. Mech Mater 209:105424.

[34] Karabulut PM, Çömez İ (2023) Continuous and discontinuous contact problem of a functionally graded orthotropic layer indented by a rigid cylindrical punch: analytical and finite element approaches. ZAMM - J Appl Math Mech Z Für Angew Math Mech 103:e202200427.

[35] Öner E, Yaylaci M, Birinci A (2014) Solution of a receding contact problem using an analytical method and a finite element method. J Mech Mater Struct 9:333–345.

[36] Yan J, Mi C, Liu Z (2019) A semianalytical and finite-element solution to the unbonded contact between a frictionless layer and an FGM-coated half-plane. Math Mech Solids 24:448–464.

[37] Yildirim B, Yilmaz KB, Comez I, Guler MA (2019) Double frictional receding contact problem for an orthotropic layer loaded by normal and tangential forces. Meccanica 54:2183–2206.

[38] Alexeyeva LA, Duishenaliyev TB, Sarsenov BT (2020) Dynamics of an elastic punch on an elastic half-plane with crack formation. Comput Math Math Phys 60:1499–1517.

[39] Babich SYu, Guz AN, Rudnitskii VB (2004) Contact problems for prestressed elastic bodies and rigid and elastic punches. Int Appl Mech 40:744–765.

[40] Babych SYu, Yarets'ka NO (2021) Contact problem for an elastic ring punch and a half-space with initial (residual) stresses*. Int Appl Mech 57:297–305.

[41] Babych SYu, Yarets'ka NO, Dehtyar SV (2023) Contact problem for half-spaces and elastic cylinder with initial (residual) stresses*. Int Appl Mech 59:442–454.

[42] Bohórquez L, Domínguez J (2005) Analysis of the elastic punch-substrate contact under fretting: monotonic and cyclic loading of the punch. Int J Mech Sci 47:388–417.

[43] Jiang X, Shao G, Zhu L (2016) Frictionless contact of an elastic punch subject to the normal load and bending moment. J Appl Mech Tech Phys 57:359–368.

[44] Polat A (2021) Examination of contact problem between functionally graded punch and functionally graded layer resting on elastic plane. Struct Eng Mech 78:135–143.

[45] Reddy JN (2003) Mechanics of laminated composite plates and shells: theory and analysis. CRC Press.